# Abstract

## Enhancing Imaging Resolution and Depth With Adaptive Optics Focal Modulation Two-Photon Microscopy

Optical microscopy is a fundamental tool for imaging biological samples and making new scientific discoveries. However, imaging resolution and imaging depth are restricted by aberrations and background noise, which result in image distortion and blur. The introduction of spatial time-variant aberrations at the focal plane (focal modulation) of a two-photon microscope with adaptive optics enabled the desired signal to be separated from the background fluorescence and scattering noise. A fast algorithm was developed to perform spectral analysis. Adaptive optics also removed system aberrations so that only photons from the very small focal region can be detected, which substantially increases image resolution and contrast.

For regular microscopy, visualization stops at about 10 microns of tissue depth. However, fluorescent microbeads up to a depth of 600 microns could be imaged in an artificial tissue sample with adaptive optics focal modulation two-photon microscopy. The measurements showed that the lateral resolution was more than doubled and the signal-to-noise ratio was improved by 7 dB at a depth of 500 microns. This novel method allows optical sectioning and near diffraction-limited spatial resolution to be achieved when imaging deep inside a highly scattering medium.

## Introduction

Optical microscopy has been a critical tool for biological discoveries and medical diagnosis ever since it was invented in seventh century. In order to investigate how a stem cell or neuron functions, or understand the dynamics of molecular interactions, visualization of live samples at molecular levels is highly desirable. Other microscopy methods, such as scanning electron microscopy and transmission electron microscopy, require preparation procedures which kill the live cells. In 2014, Eric Betzig, Stefan W. Hell, and William E. Moerner won the Nobel Prize for their work in the development of super-resolved fluorescence optical microscopy [1].

The ability to resolve small features with an optical microscope is often limited by aberrations and scattering. Optical aberrations may arise from imperfections in the optical system or may be introduced by the physical properties of the specimen. A cover slide or mounting medium quite often induces fixed aberrations while cellular motions in live tissue bring time-variant aberrations which further degrade the performance. These issues caused by aberrations can be overcome using adaptive optics, whereby aberrations are corrected using a dynamic element, such as a deformable mirror (DM).

Adaptive optics (AO) technology was originally developed to compensate the aberrations caused by atmospheric turbulence in ground-based telescopes. The successful implementation of AO in terrestrial telescopes led researchers to apply the technology for other applications such as laser beam shaping, optical communications, data storage, vision science, and microscopy [2-5].

Optical scattering further limits the image resolution and depth by randomly redirecting the propagation directions of the photons. Image quality rapidly deteriorates

as one probes deeper into thick tissues. For conventional compound and dissection optical microscopy, visualization stops at about 10 microns of tissue depth. The invention of confocal and two-photon microscopes revolutionized imaging quality and depth. In a confocal microscope, the specimen is illuminated by a focused beam and scanned point-by-point. The signal from the focal point is de-scanned and collected by a photodetector behind a confocal pinhole. Out-of-focus light is thus rejected, which removes most background noise. Two-photon microscopy further improves the imaging depth by employing two-photon excitation, which currently defines the upper limits of penetration depth for in vivo microscopy[11]. However, the imaging depth is still fundamentally restricted by the background fluorescence and scattering noise.

Many techniques such as differential-aberration and focal modulation have been recently developed for background rejection and axial resolution enhancement [6-9]. In differential-aberration microscopy, static phase aberrations are introduced in the excitation optical path. A subtraction of an aberrated image from an un-aberrated one removes background while preserving the signal. This method effectively removes random background noises, but not so much the out-of-focus fluorescence generation.

In focal modulation microscopy, optical intensity is modulated in a tight focal volume by changing optical path length difference and thus adjusting the position of the focal plane. A photodetector collects both the oscillatory and steady signals. By the separation of the oscillatory component from the background signal, out-of-focus fluorescence background is thus removed [12].

In this paper, I developed a novel technique by integrating all the advantages of adaptive optics two-photon microscopy, differential-aberration microscopy, and focal

modulation microscopy. By applying system aberration compensation and spatial time-variant aberrations at the focal plane of a two-photon microscope with adaptive optics, I effectively corrected optical system errors and suppressed both background fluorescence and scattering noise. This novel method significantly increases the imaging resolution, contrast, and depth for thick tissues. As a result, optical sectioning and near diffraction-limited spatial resolution can be achieved when imaging deep inside a highly scattering medium.

## Materials and Methods

Fig. 1 shows the schematic diagram of an Adaptive Optics Focal Modulation Two-Photon Microscope. The hardware was initially developed for an Adaptive Optics Two-Photon Microscope.

The two-photon excitation was generated by a tunable (680–1080 nm) mode-locked Ti:Sapphire laser (140 fs, 80 MHz, Chameleon Ultra II, Coherent). The intensity of the laser was modulated by an electro-optic modulator (model 350-80LA, Con optics Inc.). A deformable mirror, or DM, (Boston Micromachines) with 140 actuators and 3.5 μm of stroke was used to compensate system wavefront error or implement focal modulation phase functions for imaging enhancement. It was placed at the conjugate plane to the exit pupil of the objective, the X and Y scanners, and the wavefront sensor. The Shack–Hartmann wavefront sensor (SHWS) with a 44 × 44 element lenslet array (AOA Inc.) was used in the system for accurate wavefront measurement.

The optical system includes three telescope relay subsystems. Lenses L1 and L2 relay the DM onto the X scanner. Lenses L3 and L4 relay the X scanner conjugate to the Y scanner. Lenses L5 and L6 relay the Y scanner to the exit pupil of the objective.

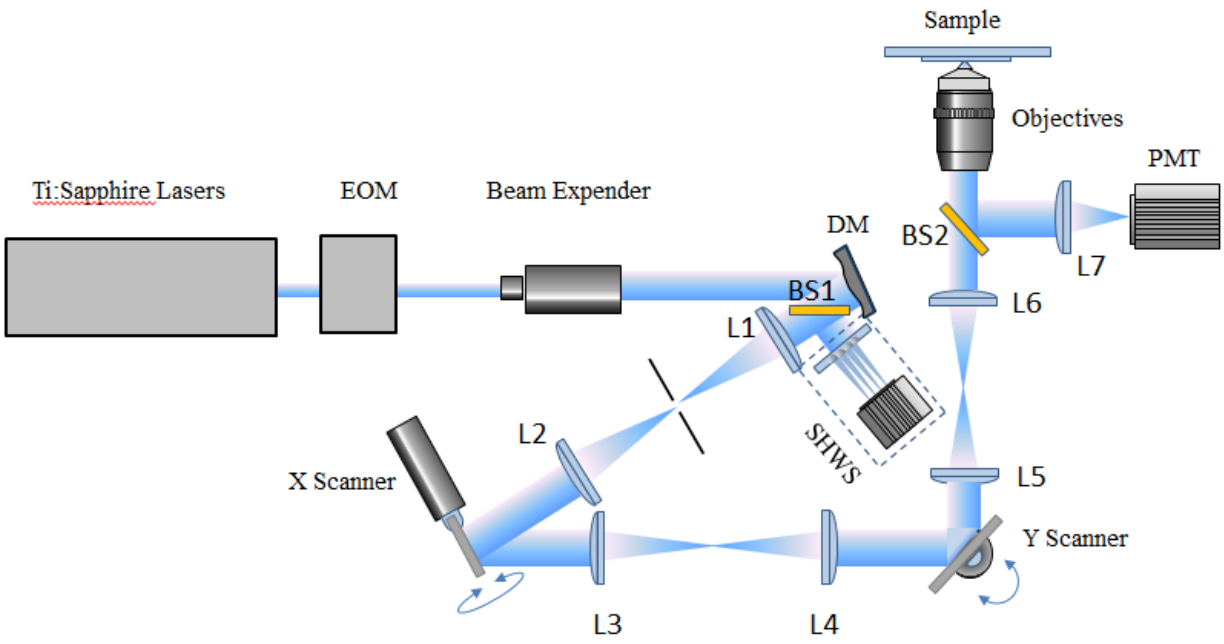


**Fig. 1** The schematic of an AO Focal Modulation Two-Photon Microscope. The main components are Ti:Sapphire laser; EOM, electro-optic modulator; beam expander; DM, deformable mirror; SHWS, Shack–Hartmann wavefront sensor; PMT, photomultiplier tube, BS, beam splitters: and Lenses (L)

A 60× water-immersion objective with a numerical aperture of 1.2 was used (Olympus Microscope) for imaging. The specimen was illuminated by a focused beam and scanned by point-by-point with the two galvo scanners (6215H, Cambridge Technology). The signal from the focal point was collected by a photomultiplier tube (PMT, H7422-20, Hamamatsu)

Due to the strict regulations of experimenting with biological samples, green fluorescent microbeads (Invitrogen, Carlsbad, CA) were used instead in imaging to demonstrate the capability of the method throughout this paper.

I utilized the existing AO Two-Photon Microscope that the lab director and the mentor developed and built in 2013. But instead of using the DM for wavefront

correction only, I applied additional spatial time-dependent phase modulation to the DM and developed algorithms to separate the background noise from the desired science signal to achieve enhanced imaging resolution, contrast, and depth.

To illustrate the principles of AO Focal Modulation Two-Photon Microscopy (AOFMTPM), the optical field at the detector $E_{image}$ can be expressed as

$$E_{image} = E_{signal} + E_{ballstic} + E_{scatter} \quad (1)$$

Where $E_{signal}$ is the desired science signal, $E_{ballstic}$ is the ballistic excitation background noise, and $E_{scatter}$ is the scattering background noise. The total phase function at the DM $P_{DM}$ can be expressed as

$$P_{DM} = P_{comp} + P_{mod} \quad (2)$$

Where $P_{comp}$ represents the wavefront error of the optical system and $P_{mod}$ represents the spatial time-variant phase modulation, which is a function of the coordinates $x$, $y$ on the DM plane and time $t$.

$$P_{mod} = P_{mod}(x, y, z_0, t) \quad (3)$$

The optical beam propagates along z direction where $z_0$ is the z coordinate of the DM plane.

Because the DM was at the conjugate plane of the objective of the microscope and the photo detector, the same phase modulation was applied to the test sample and the recorded images at the detector. The phase modulation $P_{mod}(x, y, z_0, t)$ strongly reduced the science signal at the focus ($E_{signal}$) and left the background noise generated by out-of-focus fluorescent generation ($E_{ballstic}$) and multiple scattering ($E_{scatter}$) relatively unaffected when additional phase errors were induced. Furthermore, only ballistic photons from fluorescent generation contribute to the time-variant change

in the optical field at the detector as they have well defined phase and polarization, whereas photons from multiple scatterings do not. If the oscillatory component in the detected fluorescence signal can be readily differentiated from the non-oscillatory background signal from multiple scatterings, near-focus and out-of-focus background noise from both ballistic and scattering photons can be further reduced. An algorithm utilizing the fast Fourier transform was developed to remove the background noise and keep the science signal information. A fast Fourier transform performed on the acquired images retrieves both the AC and DC signals. The DC signal represents the maximum intensity by AOFMTPM while the AC signals were used for image formation. .

Image acquisition with AOFMTPM was achieved in three steps:

1) Characterize the optical system: Measure the residual wavefront error of the optical system with the wavefront sensor, and compensate phase error with the DM. In this step, the system was used as an AO two-photon microscope.
2) Apply desired phase modulation $P_{mod}(x, y, z_0, t)$ with the DM.
3) Perform Fourier transforms and post-imaging processing

## Results, Illustration, and Discussions

1 μm green fluorescent microbeads were mixed with a 5% agarose gel and imaged to evaluate AOFMTPM in term of imaging quality improvement.

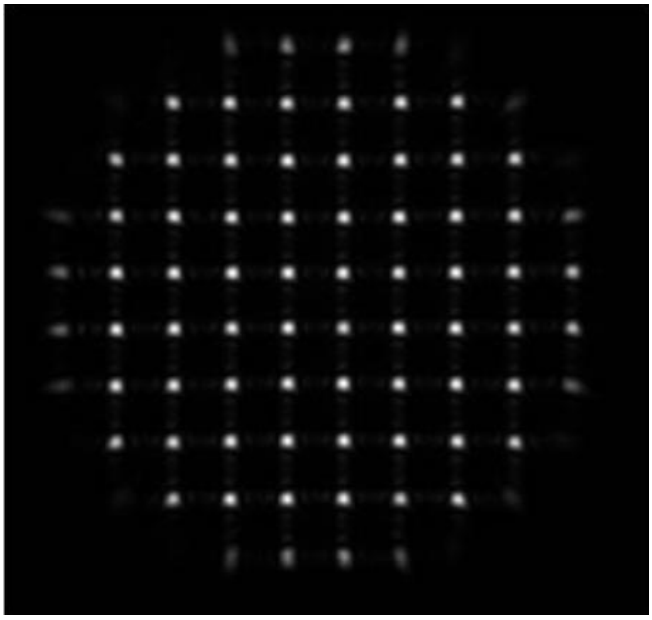

**Fig. 2** Shack-Hartmann wavefront sensor image from a microbead at the depth of 200 μm

The optical system was shown in Fig. 1. The excitation light at 900 nm was emitted by the tunable Ti:Sapphire laser, propagated to DM, relayed by three telescopes to x and y scanners and the exit pupil of the microscope objective, and finally focused on the microbeads. The fluorescence light was emitted at 530 nm at the focal region. BS2 was on a flip mount. Emitted light was reflected by BS2 and refocused to the photomultiplier tube (PMT) by lens L7 or relayed back along the excitation path to the SHWS.

Changes in the index of refraction due to tissue composition and the cover glass of the sample introduced aberrations to the optical path which would limit the resolving power of the microscope. The aberrations increase with the measurement depth. Fig. 2

shows the SHWS image from a microbead at the depth of 200 µm. The phase aberration is then calculated from the SHWS measurement. The RMS wavefront error is 0.09 µm across the whole aperture.

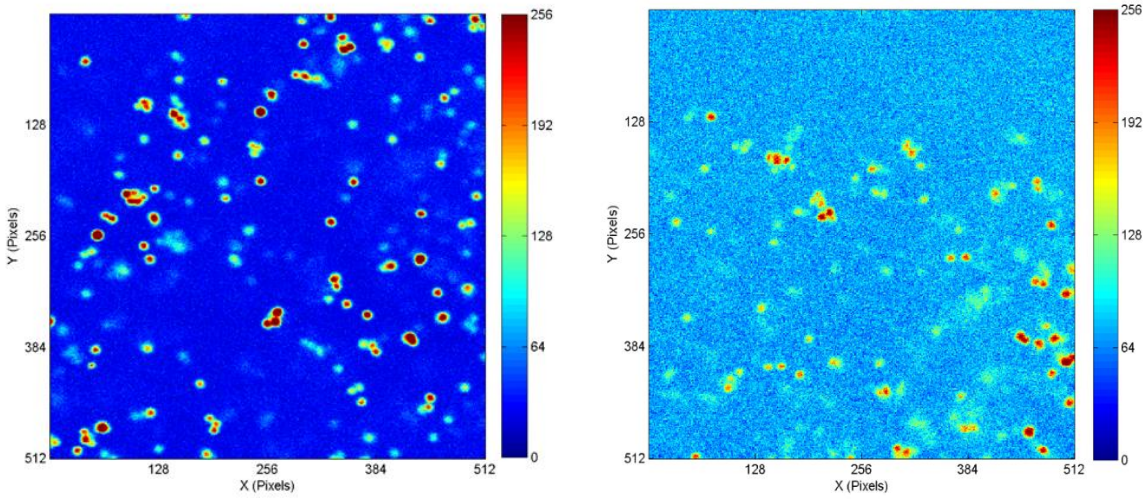


Fig. 3(a) Fig. 3(b)

**Fig. 3** shows images from a regular AO Two-Photon Microscope at depths of (a) 200 µm (b) 500 µm.

The aberration maps $P_{comp}$ at different depths were saved in the database and phase compensations were applied accordingly when imaging through different depths. Because the SHWS and DM are located on the emission and excitation paths, respectively, open-loop DM control is applied. High-speed and high-performance wavefront measurement and correction are the critical advantages of direct wavefront measurement over other sensor-less AO systems.

Fig. 3 shows the images acquired at a depth of 200 µm and 500 µm respectively after AO compensation for the wavefront errors. The laser power at the sample is 30 mW. The exposure time of a single measurement is 30 ms. The image area is 50 µm x 50 µm. Images are 8-bit and 512 x 512 pixels in size. Comparing images at depths of

200 μm and 500 μm, we can see that the intensity is drastically reduced, contrast is much worse, and background noise is substantially higher as depth increases.

I then applied additional phase modulation to the DM to suppress the background and enhance the science signal in the image. As noted by Leray and Mertz[8], there are constraints on the allowed DM-induced aberration patterns. The patterns should help to suppress the signal at the focus, while not increasing the signal in the out-of-focus area. Imposed aberration should not provoke beam defocus or tilt. They showed that a spiral pattern rather than a binary or quadrant-phase pattern has better overall performance. The choice of phase modulation pattern also depends on the sample of interest. Instead of a fixed pattern, a spiral pattern was applied over the spatial domain in which amplitude linearly increased with time and then linearly decreased with time.

$$P_{mod}(x, y, z_0, t) = A(t)\ \frac{2r\theta}{R}, \tag{4}$$

where $R$ is the aperture size of the DM, $\theta = arctan\left(\frac{y}{x}\right)$, $r = \sqrt{x^2 + y^2}$ and

$$A(t) = \begin{cases} t, & 0 < t \leq 0.5 \\ 1 - t, & 0.5 < t \leq 1 \end{cases}, \text{ where } t \text{ is the modulation time in seconds} \tag{5}$$

The sample was imaged from 200 μm to 600 μm, with a 10 μm increment in depth. 10 frames were taken in 1 second at every depth.

Fig. 4 shows the ten images at the depth of 200 μm with the phase modulation. Image 4(a) was acquired after minimizing system aberration with AO. The image has a good resolution and contrast, but possesses strong background noise from the undesirable out-of-focus fluorescent light. As the aberrations increased, the images got more blurry. The image 4(f) had the worst performance with the strongest aberration,

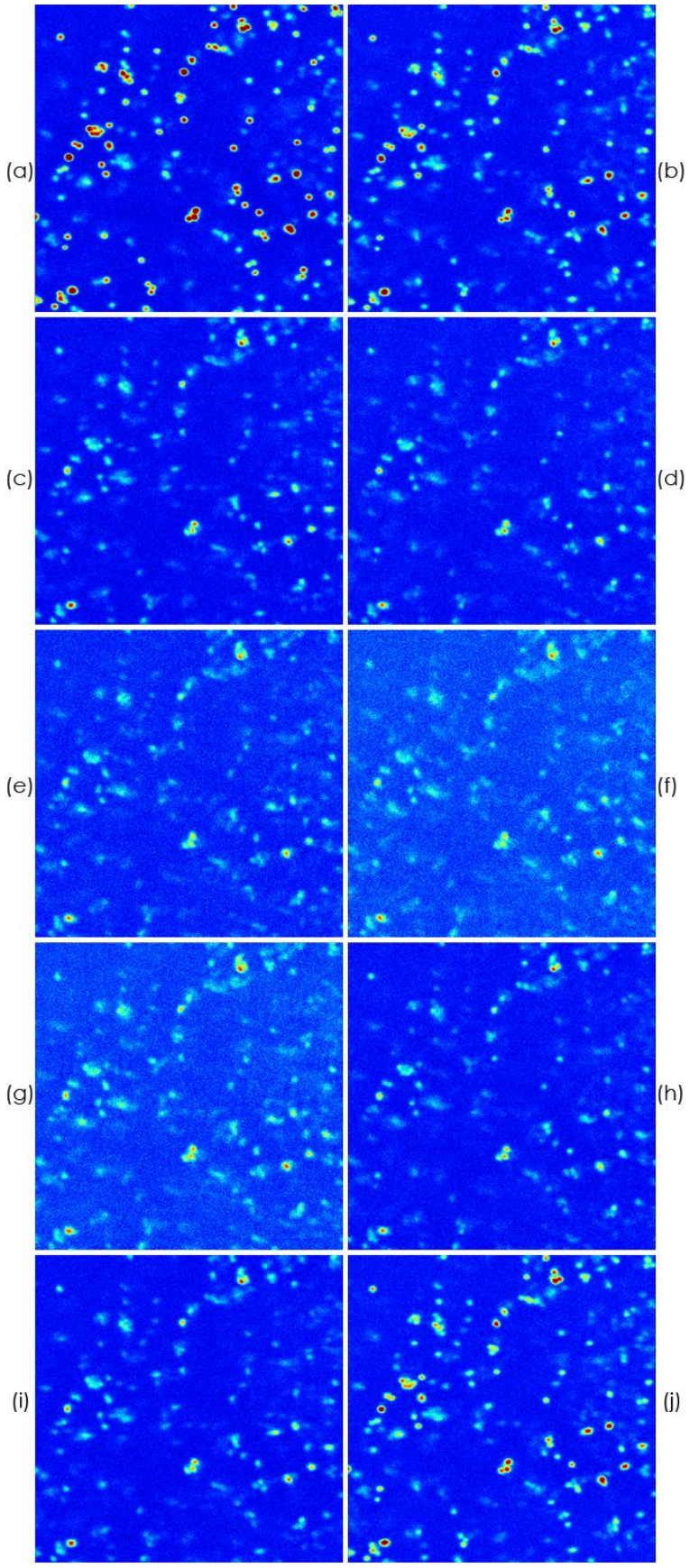


**Fig. 4** shows the ten images at the depth of 200 μm with the time-dependent phase modulation. Ten image frames were acquired at the time interval of 0.1 second from (a) to (j).

with the science signal distorted and strong scattering noise. Then, aberrations applied by the DM were gradually reduced from 4(f) to 4(j) and the phase modulation was reduced to zero, completing a full cycle of the image acquisition.

The ten frame images in Fig. 4 demonstrated that phase modulation applied by the DM strongly reduced the science signal at the focus and left the out-of-focus background noise relatively unaffected. Even though the excitation photons that reached the focal plane included both ballistic and scattered photons, only the ballistic photons from fluorescent generation contributed to the time-variant change in the optical field at the detector. This is because they have well-defined phase and polarization, while photons from multiple scatterings do not. An algorithm with a fast Fourier transform was applied to process the ten frames of images so that the oscillatory component (science signal) and non-oscillatory components (background noise) are separated.

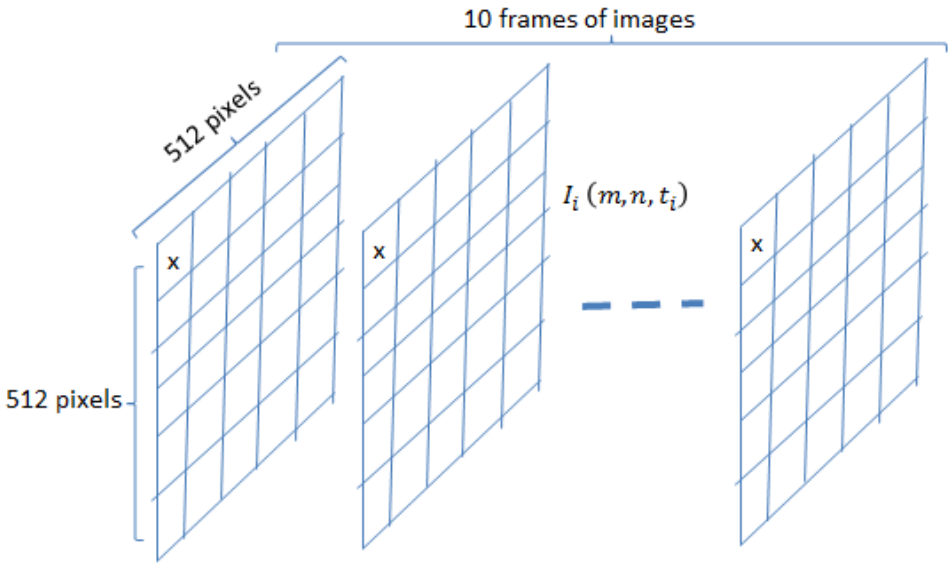


**Fig. 5** Schematic to demonstrate how the images are recorded, addressed, and programmed for post-imaging processing.

The schematic diagram in Fig. 5 illustrates how the algorithm was implemented for post-imaging signal processing. Each frame consists of 512 x 512 pixels. The intensity of each image is represented by $I_i\,(m,n,t_i)$, where $i$ is the frame number, $m,n$ address the location of the pixels, and $t$ is the time. Fast Fourier transforms were performed over the series of $I_i\,(m,n,t_i)$ where $i$ ranges from 1 to 10, and the first AC component, which is associated with the sampling frequency, was saved. All the other terms including the DC signal and higher-order AC components are removed from the image. This process removes the undesired out-of-focus fluorescent background and scattering noise.

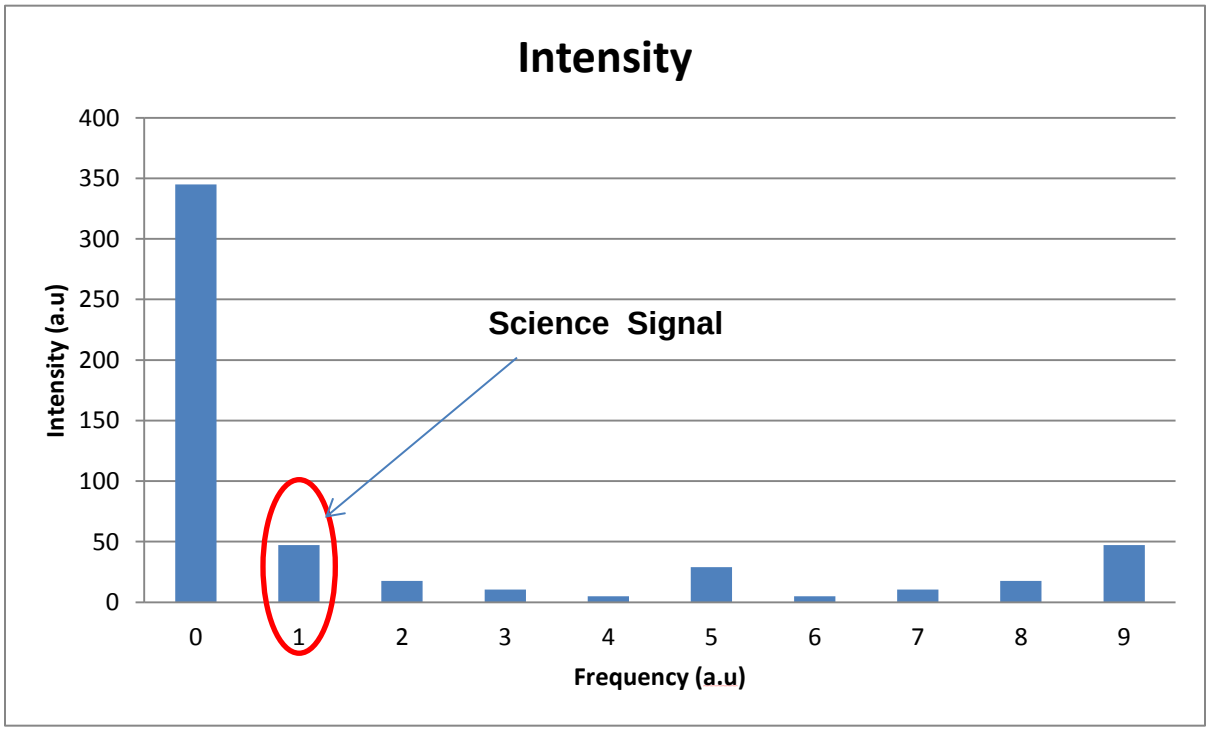


**Fig. 6**. Fourier transform of ten images at one pixel. Only the oscillation signal associated with the first order of the sampling frequency is saved. This signal is the desired science signal from the test sample.

The algorithm was first developed with a MATLAB prototype. Reading previously saved images from the hard disk, the MATLAB program was not only significantly

slower than other languages, but also possessed too much overhead, taking a whole 15 seconds of processing time. A language change to C++ enabled a more streamlined process with the imaging system, which also used C++. Computation is faster in C++, which yielded a processing time of 2.8 seconds. Furthermore, the switch permitted the skipping of a costly step, saving images to and reading images from the hard disk. The Fourier analysis process could thus be integrated directly into the system, allowing camera input to be used directly from memory and shaving another 0.5 seconds off, for a final C++ time of 2.3 seconds. However, OpenCV, the C++ library used for image processing, still required considerable overhead – the Fourier transformation cost was less than half the total time.

In order to improve the constant matrix resizing, type conversions, and expensive arithmetic operations, a GPU (graphics processing unit) was used to perform the spectral analysis. The use of an NVIDIA GeForce GTX 770 card and the NVIDIA GPU language, CUDA, enabled parallel processing with over a hundred thousand parallel threads, used for both Fourier transformations and self-built, optimized arithmetic manipulation functions. This sped up processing to 0.5 seconds. The simulation and imaging processing speed are very important when applying the algorithm to observe live, dynamic biological tissues.

Fig. 7(a) and (b) compare the images without and with AOFMTPM. This is a section of the whole image from Fig. 4. Resolution and contrast were significantly improved with AOFMTPM. The random noise was substantially suppressed. Background fluorescence generation can be seen from the circled regions in 7(a), but with AOFMTPM, these undesirable photons were removed, as demonstrated in Fig.

7(b). Fig. 7(c) shows a section slice through a microbead image. Lateral resolution demonstrates the resolving power of a microscope and can be quantified by the full width at half maximum (FWHM) of the beads. The FWHM sizes of the beads were 9.6 and 4.9 pixels respectively, without and with AOFMTPM. The ratio of the two is 1.96, so the lateral resolution is nearly doubled.

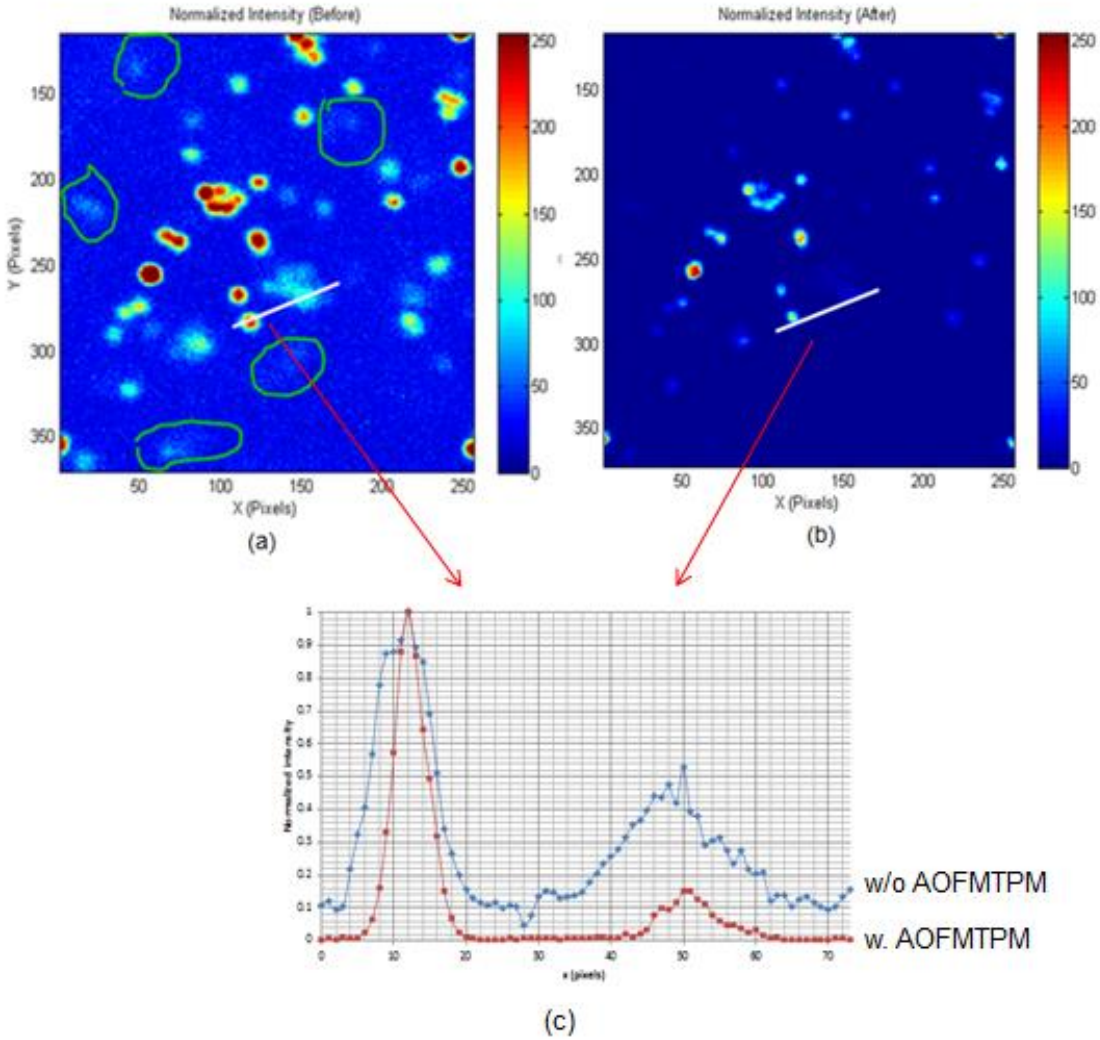


**Fig. 7** At 200 μm (a) image without AOFMTPM (b) Image with AOFMTPM (c) Section slice of a microbead

As I imaged structures deeper in the sample, more out-of-focus fluorescent microbeads were illuminated. The random scattering was more severe due to the undesired emitted background, as shown in Fig. 3(b). AOFMTPM is more effective in suppressing the noise as demonstrated in Fig. 8.

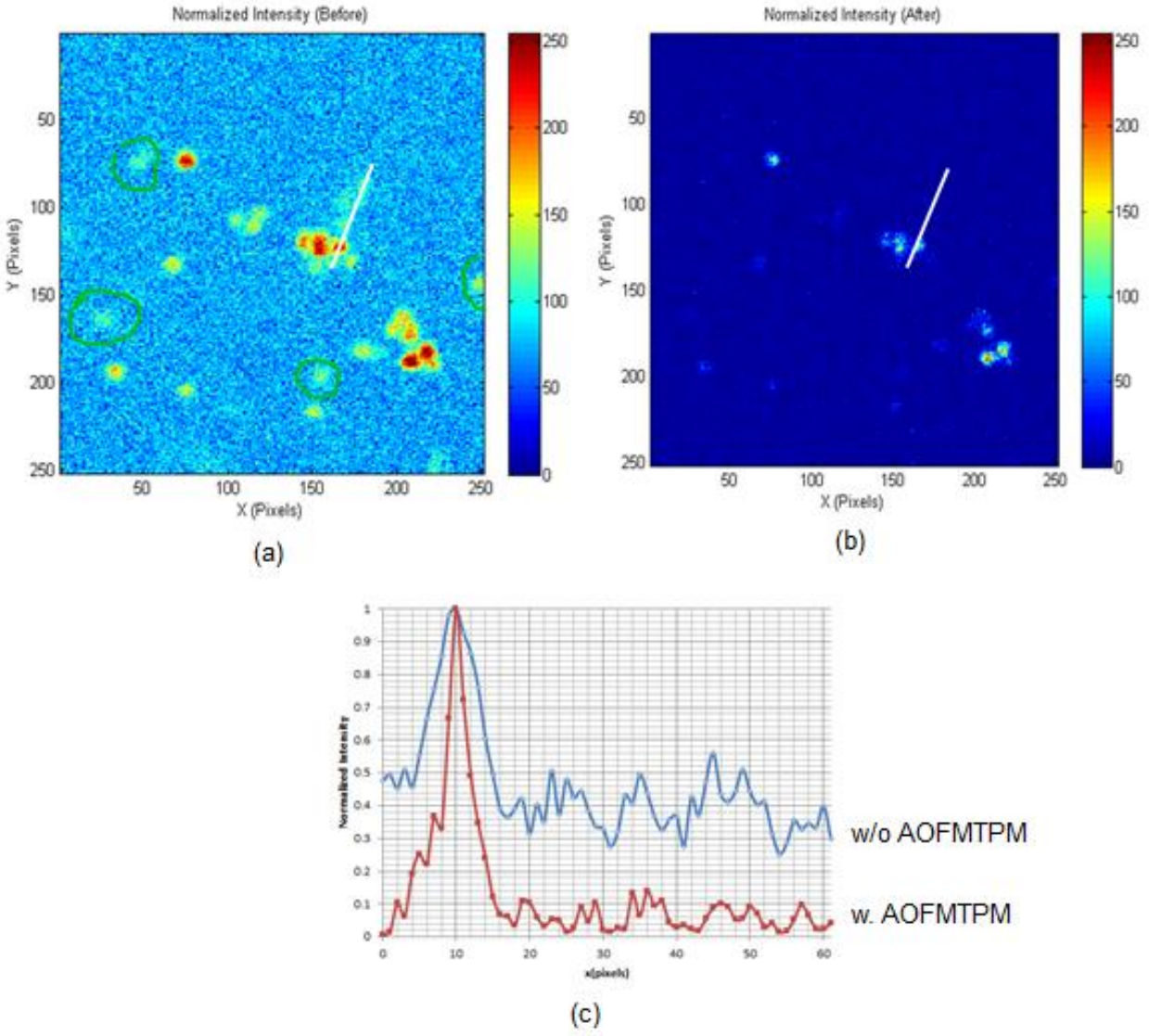


**Fig. 8** At 500 μm (a) Image without AOFMTPM (b) Image with AOFMTPM (c) Section slice of a microbead

Both the out-of-focus fluorescent and the random scattering noise are significantly reduced. The image background noise in the highlighted areas in the left pictures was almost gone after applying the improved imaging method. The results showed that the final images are much sharper. The signal-to-noise ratio (SNR) were 28.7dB and 35.8dB, respectively, without or with AOFMTPM at the depth of 500 μm. The SNR was improved by 7.1 dB with AOFMTPM method, with an RMS error of 0.4 dB. The FWHM sizes of the beads were 9.8 and 3.7 pixels respectively, without and with AOFMTPM in Fig. 8(c). The ratio of the FWHMs between the two is 2.65. Ten beads were measured at the same depth, and the average ratio is 2.1. So the lateral resolution is more than doubled with the AOFMTPM method.

## Conclusions and Future work

I have developed and experimentally demonstrated a novel microscopy method for deep tissue imaging by introducing spatial time-variant aberrations at the focal plane of a two-photon microscope with adaptive optics. The background fluorescence and scattering noise were effectively suppressed by this method. Fluorescent microbeads up to a depth of 600 microns in an artificial tissue sample were successfully measured through a highly scattering medium. The measurements showed that the lateral resolution was doubled and signal-to-noise ratio was improved by 7 dB at a depth of 500 microns. I developed a fast algorithm with CUDA to separate the desired science signal from the background noise, which reduced the imaging processing time of a 512 x 512 image from 15 seconds to 0.5 seconds.

I would like to explore future work in several areas:

1) Investigate the phase modulation functions and find the function which optimizes the signal-to-noise ratio and provides the best image
2) Explore the depth limitation of this method with biological tissues
3) Further improve the speed of data acquisition and data analysis for real-time imaging of a live tissue, possibility for video
4) Develop a 3D reconstruction tool for a 3D illustration of the tissue sample

## References


1) Nobelprize.org,http://www.nobelprize.org/nobel_prizes/chemistry/laureates/2014

2) “Optical and Digital Image Processing”, G. Cristobal, P. Schelkens, and H. Thienpont, Wiley, (2011)

3) A. Roorda, F. Boria, W. Donnelly, H. Queener, T. Hebert, and M. Campbell, “Adaptive optics scanning laser ophthalmoscopy”, Opt. Express **10**(9), 405-412, (2002)

4) X. Tao, Z. Dean, C. Chien, O. Azucena, D. Bodington and J. Kubby, “Shack-Hartmann wavefront sensing using interferometric focusing of light onto guide-stars”, Opt. Express **21**(25), 31282-31292 (2013)

5) X. Tao, A. Norton, M. Kissel, O. Azucena, and J. Kubby, “Adaptive optical two-photon microscopy using autofluorescent guide stars”, Opt. Lett., **38**(23), 5075-5078, (2013)

6) C. Stockbridge, Y. Lu, J. Moore, S. Hoffman, R. Paxman, K. Toussaint, and T. Bifano, “Focusing through dynamic scattering media,” Opt. Express **20**(14), 15086–15092 (2012).

7) M. Cui, “A high speed wavefront determination method based on spatial frequency modulations for focusing light through random scattering media,” Opt. Express **19**(4), 2989–2995 (2011).

8) A. Leray, K. Lillis, and J. Mertz, “Enhanced background rejections in thick tissue with differential-aberration two-photon microscopy”, Bio. Phy. J., 94, 1449-1458 (2008)

9) D. Conkey, A. Caravaca-Aguirra, and E. Piestun, “High-speed scattering medium characterization with application to focusing light through turbid media”, Opt. Express **20**(2), 1733-1740 (2012)

10) N. Chen, C. Wong, and C. Sheppard, “Focal modulation microscopy”, Opt. Express **16** (23), 18747-18769 (2008)

11) W. Denk, J.H. Strickler and W.W. Webb, “Two-photon laser scanning fluorescence microscopy”, *Science* 248, 73–76 (1990).

12) J. Goodman, “Introduction to Fourier Optics”, Roberts & Company Publishers, (2005).